THE JOURNAL OF PHYSICAL CHEMISTRY B

Article

pubs.acs.org/JPCB

Peptide–Microgel Interactions in the Strong Coupling Regime

Per Hansson,* Helena Bysell, Ronja Månsson, and Martin Malmsten

Department of Pharmacy, Uppsala University, P.O. Box 580, SE-751 23 Uppsala, Sweden

ABSTRACT: The interaction between lightly cross-linked poly(acrylic acid) microgels and oppositely charged peptides was investigated as a function of peptide length, charge density, pH, and salt concentration, with emphasis on the strong coupling regime at high charge contrast. By micromanipulator-assisted light microscopy, the equilibrium volume response of single microgel particles upon oligolysine and oligo(lysine/alanine) absorption could be monitored in a controlled fashion. Results show that microgel deswelling, caused by peptide binding and network neutralization, increases with peptide length ($3 < 5 < 10$) and charge density (30% < 50% < 100%). Furthermore, oligomer-induced microgel deswelling was more pronounced at pH 5 than at pH 8, reflecting the lower network charge density in the former case (pK_a for the isolated acrylic acid ≈4.7). In order to describe these highly coupled systems, a model was developed, in which counterion/peptide-mediated electrostatic attraction between the network chains is described using an exponential force law, and the network elasticity by the inverse Langevin theory. The model was used to calculate the composition of microgels in contact with reservoir solutions of peptides and simple electrolytes. At high electrostatic coupling, the calculated swelling curves were found to display first-order phase transition behavior. The model was demonstrated to capture pH- and electrolyte-dependent microgel swelling, as well as effects of peptide length and charge density on microgel deswelling. The analysis demonstrated that the peptide charge (length), rather than the peptide charge density, determines microgel deswelling. Furthermore, a transition between continuous and discrete network collapse was identified, consistent with experimental results in the present investigations, as well as with results from the literature on microgel deswelling caused by multivalent cations.

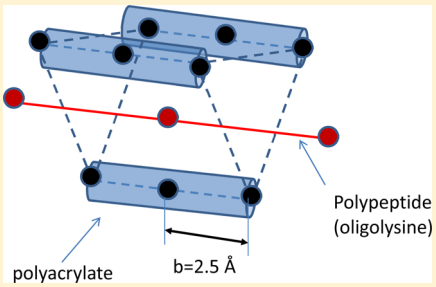

INTRODUCTION

Due to their frequently low cross-linking density, microgels are able to drastically change their volume in response to changes in their environment, e.g., pH, ionic strength, temperature, and presence of specific ions and metabolites, but also to directed biodegradation and external fields.[1−5] As a result of this, microgels are able to incorporate host molecules and to release these in a responsive manner, and offer opportunities as drug delivery systems and functional biomaterials.[1−3] This is of particular interest for peptide and protein drugs, since these can be incorporated in microgels with limited loss in native conformation and biological activity.[3,6]

The interaction between polyelectrolytes/peptides/proteins and oppositely charged microgels depends on factors such as peptide and microgel charge density, pH, and ionic strength.[7−12] At low peptide and microgel charge densities and/or high ionic strength, non-electrostatic contributions become increasingly important.[9,13−15] These effects have been demonstrated to depend on peptide length,[8,10] oligomerization/aggregation,[13,16] and peptide secondary structure.[17] Of particular relevance for the present investigation, effects of peptide length and charge density on microgel interactions were previously investigated in a couple of studies. Thus, for a series of polylysine homopolypeptides of different molecular weight, a transition in peptide distribution within poly(acrylic acid) microgels was demonstrated at a critical peptide length.[8] Below the critical peptide length, which depends on microgel charge density, peptides were able to distribute throughout microgels, whereas peptides larger than this were unable to diffuse through the contracting microgel network, thereby forming a core–shell structure. In addition, the interaction between microgels and antimicrobial peptides of different length was previously investigated for peptides of the type $(AKKAKA)_n$ $(1 \le n \le 4)$ $(ARKKAAKA)_n$ $(1 \le n \le 3)$ (A and K being alanine and lysine, respectively), demonstrating increased microgel deswelling and reduced desorption at high ionic strength with increasing peptide length.[10] However, while valuable experimental observations could be made in these previous studies, no theoretical analysis was possible due to the complexity of the systems investigated.

In an attempt to address the effect of peptide charge density on peptide–microgel interactions, we previously investigated a series of monodisperse peptides of varying charge density, charge distribution, and hydrophobicity (both the latter at constant net charge). Modeling these effects by a modified Flory–Rhener theory, without consideration of electrostatic energy, in combination with a model of mass transport,[18] good agreement was found regarding effects of peptide charge density on microgel deswelling kinetics.[9] While the latter work was thus able to describe the experimental results regarding peptide-induced microgel deswelling, the approach taken is only applicable to low charge density systems. Highly charged gel systems, on the other hand, where the strong electrostatic

Received: June 21, 2012
Published: August 10, 2012

coupling and ion correlation effects dominate, require a more detailed description with Coulomb interactions taken into account.[19−23] Here, we therefore use a new simple approach to calculating the electrostatic energy of polyelectrolyte systems based on the "strong coupling" theory by Moreira and Netz[24] but adopting an exponential force law of the ion correlation attraction. When combined with an elastic theory of networks, this provides us with a description suitable for semiquantitative modeling of charged networks in systems of largely varying electrostatic coupling strength.

Given the importance of highly charged systems in various drug delivery systems in particular (peptide, DNA, and siRNA), we here investigate such highly charged systems for a series of lysine oligopeptides (KKK (K3), KKKKK (K5), and KKKKKKKKKK (K10)) and lysine (K)/alanine (A) copeptides of varying charge density (K5A5, KAKAKAKAKA; K3A7, KAAAKAAAAK) in lightly cross-linked poly(acrylic acid) microgels, focusing on effects of oligomer length, charge density, pH, and ionic strength. By using micromanipulator-assisted light microscopy, the equilibrium volume change of single microgel particles in response to oligomer absorption of increasing concentration and length could be successfully monitored. Experimental results obtained on microgel behavior in the absence and presence of the lysine oligomers are compared to results from theoretical modeling.

THEORY

In this section, we first derive expressions for the interaction between two charged planar walls in the presence of counterions. The result is then generalized to cylindrical polyelectrolytes and used in the formulation of a theory of polyelectrolyte networks.

Planar Systems. The electrostatic interactions are conveniently described using two characteristic length scales, the Bjerrum length (l_B) and the Gouy−Chapman length (l_{GC}), measuring the distances between two elementary charges and between wall and counterion, respectively, at which the thermal energy k_BT equals the Coulomb energy:

$$l_B = \frac{e^2}{4\pi\varepsilon_0\varepsilon_r k_B T} \tag{1}$$

$$l_{GC} = \frac{e}{2\pi z\sigma l_B} \tag{2}$$

where e is the elementary charge, ε_0 is the permittivity of vacuum, ε_r is the dielectric constant of the medium, k_B is Boltzmann's constant, T is the absolute temperature, z is the counterion valency, and σ is the charge density of the wall. For the special case of two parallel, similarly charged walls separated by a medium containing point-like counterions only, the exact description is fully characterized by two dimensionless parameters.[25] These can be defined as

$$\lambda = \frac{L}{l_{GC}} \tag{3}$$

$$\Xi = \frac{z^2 l_B}{l_{GC}} \tag{4}$$

where L is half the distance between walls. Figure 1a shows the reduced pressure P between the walls as a function of λ for different electrostatic coupling strengths (Ξ) according to Monte Carlo simulations by Moreira and Netz.[24] P is defined as

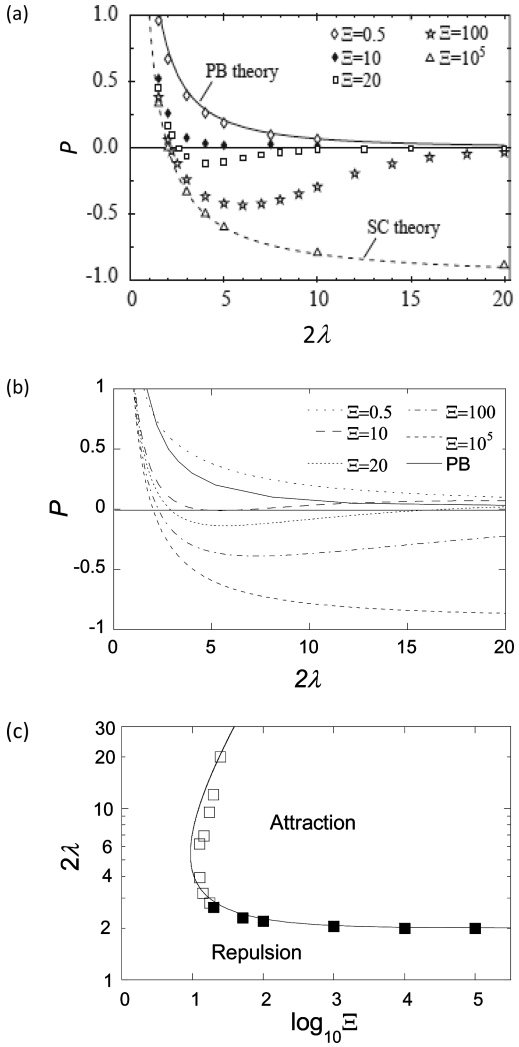

Figure 1. (a) MC simulation results showing reduced pressure (P) plotted vs distance (2λ) between two charged planar walls in the presence of point-like counterions; coupling strengths (Ξ) as indicated. Data taken from ref 24. Lines show the results from SC theory (dashed) and PB theory (solid). (b) P as a function of 2λ calculated from eq 7 for Ξ as indicated, and the result from PB theory. (c) Interaction map for system point-like ions between planar walls. The separation (2λ) where the pressure is zero is plotted vs $\log_{10}\Xi$. The line shows the boundary between attractive and repulsive regions calculated from eq 7. Symbols are the corresponding results from MC simulations,[24] where filled symbols are stable states and open symbols are unstable or metastable states.

$$P = \frac{p}{2\pi l_B k_B T(\sigma/e)^2} \tag{5}$$

where p is the actual (osmotic) pressure. In the weak coupling regime ($\Xi \ll 1$), the exact result is well described by the mean-field Poisson−Boltzmann (PB) theory, according to which the reduced pressure is given by $P_{PB} = \Lambda$; $\sqrt{\Lambda}\tan(\lambda\sqrt{\Lambda}) = 1$.[26] P_{PB} is always positive and decreases monotonically with increasing distance between the walls; in the limit $L \gg \lambda$, $P_{PB} \approx (\pi/2\lambda)^2$. In conflict with that, the interaction becomes attractive in the strong coupling (SC) regime ($\Xi \gg 1$) where P at sufficiently small wall separations approaches the limiting law:[24]

dx.doi.org/10.1021/jp306121h | J. Phys. Chem. B 2012, 116, 10964−10975

$$P_{SC} = \frac{1}{\lambda} - 1 \tag{6}$$

For comparison, the exact pressure is given by the contact value theorem (CT),[27,28] which in the case of one type of counterion only and with the present notations can be written $P_{CT} = (C_0/C_{av})(1/\lambda) - 1$, where C_0 is the counterion concentration in contact with the walls and C_{av} is the average concentration. Thus, CT applied to a uniform distribution of ions gives the pressure in the SC theory.

The first term on the rhs in eq 6 is the repulsive contribution from confining the counterions between the walls. The second term describes the attraction resulting from the wall−wall and wall−counterion Coulomb interactions. The attraction is a consequence of the lateral repulsion between the counterions and becomes important when the distance between counterions is larger than the separation between the walls. Each counterion is then effectively confined to an electroneutral "correlation cell" where it attracts an area of bare charge on both walls.[25,29] The constant contribution of −1 is the resulting reduced pressure in the limit as $\Xi \to \infty$. In essence, the ion−wall interaction becomes independent of the position of the ion in the correlation cell.

For small wall separations, eq 6 works reasonably well for coupling strengths down to $\Xi = 20$ (Figure 1a). In this range, the distance at which attraction and repulsion balance each other ($P = 0$) deviates little from the SC asymptotic limiting value $2L = 2L_{GC}$ ($\lambda = 1$). At larger distances and lower Ξ, the SC theory breaks down altogether and there is a wide Ξ range where neither PB and SC applies.

The description at intermediate coupling strengths can be improved by adopting an exponential force law for the correlation attraction, thereby replacing the second term in eq 6 by $-e^{-L/L_C}$, where L_C is a decay length. The correlation attraction is strong when the average lateral distance between counterions is larger than the separation ($2L$) between the walls.[25] In this range, each counterion can be considered to attract a surface area equal to (the absolute value of) $ze/(2\sigma)$ on both walls, so the average distance between counterions can be taken as $(ze/2\sigma)^{1/2} = l_{GC}(\Xi\pi)^{1/2}$, where we have used eqs 1, 2, and 4. Since L is half the distance between the walls, we put $L_C = l_{GC}(\Xi\pi)^{1/2}/2$, so that

$$P_C = \frac{1}{\lambda} - e^{-2\lambda/\sqrt{\Xi\pi}} \tag{7}$$

The result obtained from eq 7 is shown in Figure 1b. At the highest coupling strength, where the exponent becomes close to zero, and in the limit as $\lambda \to 0$, the result coincides with that of the SC theory (eq 6). At the weakest coupling strength, the result is in fairly good agreement with the exact result and the PB theory at small λ. At larger separations, however, the pressure is overestimated due to the assumption of a uniform distribution of ions when evaluating the entropy. For all finite values of Ξ, the pressure becomes repulsive at sufficiently large separation (not shown); however, the pressure in this range decreases as λ^{-1}, not λ^{-2} as in PB. For $\Xi > 4.3$, jump transitions take place between two separations corresponding to phase transitions in the thermodynamic limit. With increasing Ξ, the corresponding wall−wall separations (2λ) approach asymptotically the values 2 and infinity, respectively.

Figure 1c shows the separation where $P = 0$ as a function of $\log_{10}\Xi$ calculated from eq 7; solid line. Shown are also the corresponding data from MC simulations,[24] where filled symbols are stable states and open symbols are unstable or metastable states. The crossover from a pressure positive at all separations to the appearance of negative pressures takes place at $\Xi \approx 9.4$ (eq 7) and $\Xi \approx 12$ (MC). The boundary between attractive and repulsive regions is remarkably well predicted by eq 7. In this respect, it clearly represents an improvement for $\Xi < 20$ compared to the results from SC expansions including corrections up to first order.[24,30] Recently, powerful methods of interpolation between weak (PB) and SC regimes,[31,32] based on the notion of a correlation hole,[33,34] have been developed, providing good agreement with MC simulations for the full range of electrostatic coupling, both regarding ionic density profiles and pressure between planar walls. However, these methods, being computationally highly demanding, are less attractive in the present context.

The work per area of separating the walls consistent with the exponential force law is $(\sigma^2/2\varepsilon_0\varepsilon_r)L_C(1 - e^{-L/L_C})$. At short separation ($L \ll L_C$), this can be approximated by $\sigma^2 L/2\varepsilon_0\varepsilon_r$, which is the expression for the energy in the SC theory. At large separation ($L \gg L_C$), the energy becomes $\sigma^2 L_C/2\varepsilon_0\varepsilon_r$. These expressions have the form of the energy of a capacitor. Thus, the increase of the electrostatic energy per wall on increasing the separation from contact to infinity is equal to that of increasing the separation of a capacitor from zero to L_C. In the PB theory, the electrostatic energy per area of a single wall is $\sigma^2 l_{GC}/2\varepsilon_0\varepsilon_r$, i.e., the energy of a capacitor of one Gouy−Chapman length (corresponding to 1 k_BT per counterion). It can be noted that with $L_C \sim l_{GC}\sqrt{\Xi}$, as in eq 7, the PB limiting value is approached when the coupling parameter is reduced to the order of unity. On the other hand, at high electrostatic coupling, the energy per wall exceeds the PB value.

It can be concluded that in the SC theory a system of two planar walls behaves effectively as a set of two capacitors, one on each side of the mid plane, with the counterions forming a layer of smeared out charge positioned a distance L from the wall. With the exponential force law, each side of the midplane also behaves effectively as a capacitor but with the capacitor length decaying toward a finite value with increasing distance between the walls. Thus, the energy in both models can be written $(\sigma^2/2\varepsilon_0\varepsilon_r)y_pL$, where in the former y_p is a constant equal to 1 and in the latter $y_p = (L_C/L)(1 - e^{-L/L_C})$, which can be seen as a correction function. In the next section, this concept will be extended to linear polyelectrolytes.

Linear Polyelectrolytes. The swelling in water of charge stoichiometric complexes of linear polyions of opposite charge is typically low but depends on, e.g., the flexibility, degree of polymerization, and charge density of the chains. In a sufficiently dense state, even highly flexible polyion chains should become aligned on some length scale due to mutual repulsion. Of special interest here are complexes between poly(acrylic acid) (PA) and linear cationic peptides. Consider a hexagonal arrangement of (linear) PA chains and divide the space between them into parts of equal volume, as illustrated in Figure 2a. In such an element of length $2b$, where b is the linear separation of charges for PA (=2.5 Å for fully dissociated PA[35]), charge neutrality requires that there must be on average one positive charge. Incidentally, the separation of charges along some of the peptides in this work (K3, K5, K10) is 5 Å, meaning that each volume element contains on average one peptide segment (Figure 2b). For the peptides with lower charge density, there will still be one peptide charge per volume element but at a larger volume fraction of peptide. The picture is highly idealized, of course, and other configurations may have

dx.doi.org/10.1021/jp306121h | J. Phys. Chem. B 2012, 116, 10964−10975

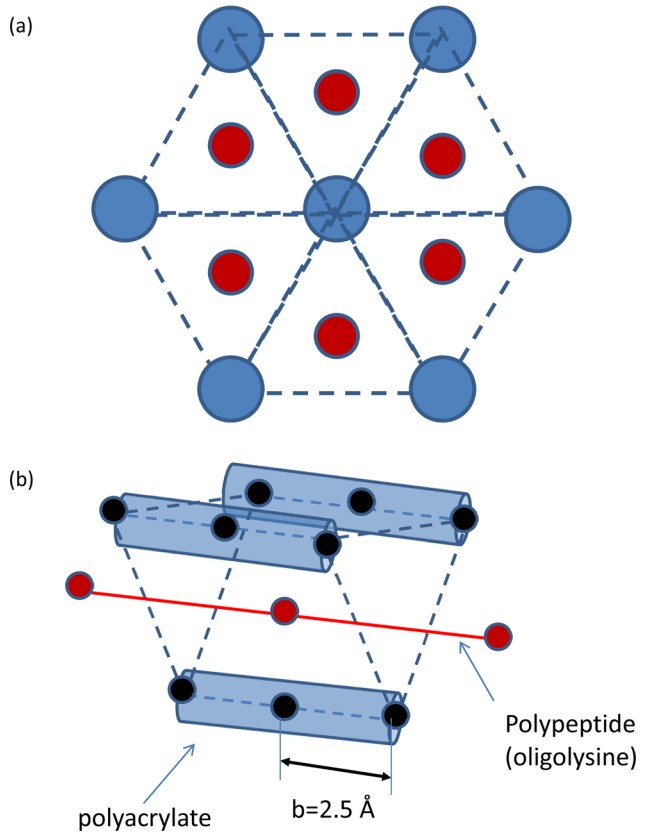

Figure 2. (a) Hexagonal arrangement of polyion chains (blue) surrounded by peptides (red). (b) Side view of a volume element ("correlation cell") of length 2b containing one peptide charge. The peptide chain is arbitrarily positioned in the center of the volume element.

lower electrostatic energy, but it shows that a peptide charge interacts with the bare charge of more than one PA chain. This gives rise to an attraction, similar to the attraction due to correlated counterions between flat surfaces. Note that the peptide charges are intrinsically correlated due to the stiffness of the peptide backbone. In addition to that, there is the *correlation between the peptide chains*. In the SC regime in the planar case, the Coulomb energy is independent of the position of the counterion in the correlation cell. In the present case, even if each peptide chain would be confined to an independent cell, the energy would depend on the position. Neglecting such details, it is clear that in a sufficiently dense state a PA chain should have as nearest neighbors a layer of peptides (Figure 2a). Upon swelling of the structure, the average separation between PA and peptide charges will initially increase, and therefore so will the electrostatic energy. However, at larger distances between the PA chains, the peptides will to a lesser extent be shared between different PA chains, and at sufficiently large separation, a large fraction of the peptide molecules will remain in close vicinity to a single PA chain. By analogy with the planar case, it will be assumed that the variation of the electrostatic energy in the process is subsumed by the expression for the energy of a *cylindrical* capacitor with the separation between the charged surfaces increasing asymptotically to a finite value with an appropriate rate. In the latter respect, our approach differs from that by Leal et al.[36] and Biesheuvel et al.,[37] respectively, who calculated the electrostatic free energy in systems of cylindrical polyelectrolytes of opposite charge by solving the Poisson–Boltzmann equation.

We adopt a cylindrical cell model with a polyion chain (here PA) described as a charge cylinder of radius r in the center surrounded by an aqueous layer of thickness L containing the peptide. The electrostatic energy per area per charge may be written:

$$\frac{E}{\text{area}} = \frac{\sigma^2 r}{2\varepsilon_0\varepsilon_r}\ln\left(1 + \frac{y_c L}{r}\right) \tag{8}$$

For $y_c = 1$, this is the energy of a cylindrical capacitor with separation L, which diverges with increasing separation. In the most densely packed state, the average nearest distance between correlated peptide chains would be $\sim 2\pi d/6 \approx d$, where d is the shortest center–center distance between the peptide and polyion chains. As in the planar case, the attraction is expected to be strong when the distance between the PA chains is of order d or shorter. For a cylindrical polyion surrounded by line charges, the corresponding distance would be the radius of the cylinder. In general, the Gouy–Chapman length can be taken as a measure of the thickness of the double layer formed by point-like counterions, and for charged cylinders $l_{GC} \sim rb$. Similar to the planar case, we propose, as an approximation, that the decay length of the correlation attraction depends on r in such a way that $y_c L = y_0 r(1 - e^{-L/y_0 r})$, where y_0 is a parameter related to b; see below. At small separation ($L \ll r$), $y_c L \approx L$ and $E/\text{area} \approx \sigma^2 L/2\varepsilon_0\varepsilon_r$ as in the planar case. At large separation ($L \gg r$), $y_c L \approx y_0 r$ and $E/\text{area} \approx (\sigma^2 r/2\varepsilon_0\varepsilon_r)\ln(1 + y_0)$. The contribution from eq 8 to the osmotic pressure becomes

$$\Pi_{el} = -\frac{k_B T\xi e^{-L/y_0 r}}{2\pi r b(r + L)(1 + y_0(1 - e^{-L/y_0 r}))} \tag{9}$$

where $\xi = l_B/b$ is the Manning parameter. The contribution to the chemical potential of the polyion (per charge) becomes

$$\mu_p^{el} = k_B T\xi\ln(1 + y_0(1 - e^{-L/y_0 r})) + \pi b L(2r + L)\Pi_{el} \tag{10}$$

It will be assumed that eqs 9 and 10 are applicable also in the presence of a simple monovalent salt. In the general case, this would be a poor assumption. However, in the case of phase separation from a dilute polyelectrolyte solution, it may be quite realistic. Thus, in the dense phase, the dominating counterion to the polyion will be the peptide (due to entropy) and, even for small deviations from peptide/polyion charge equivalence, salt will be excluded from the phase (Donnan effect). In the present systems, phase separation is induced already at low peptide concentrations where the simple ions are the dominating counterions to the polyion. Thus, the transition from the dense to the dilute state is accompanied by an exchange of polyion counterion from peptide to monovalent ion, a process leading to swelling and an increased electrostatic energy of the polyion. To handle this, eq 10, which in the limit of infinite dilution becomes $\mu_p^{el} = k_B T\xi\ln(1 + y_0)$, will be fitted, with y_0 as a parameter, to give convergence with the PB theory for a cylindrical polyion at infinite dilution in a 1:1 salt solution.[38]

Gel Model. Consider a negatively charged polymer network in equilibrium with an aqueous liquid solution reservoir containing a mixture of monovalent ions (+/−) and cationic peptides of charge number Z. Let C_p^* be the concentration of

dx.doi.org/10.1021/jp306121h | J. Phys. Chem. B 2012, 116, 10964–10975

polymer chain segments in a reference state of the network. In a swollen state (C_p), the contribution to the osmotic pressure Π from deforming the network is calculated using an approximation to the inverse Langevin theory of rubber elasticity:[39,40]

$$\frac{\Pi_{def}}{RT} = \frac{C_p}{xs}\left(\frac{1}{2} - \omega^2 - \frac{3\omega^4}{5s} - \frac{99\omega^6}{175s^2} - \frac{513\omega^8}{875s^3}\right) \quad (11)$$

where R is the ideal gas constant, s is the number of statistical segments between cross-links, x is the number of monomer units in a statistical segment, and ω is the deformation ratio in the free-swelling directions. For an isotropic deformation $\omega = (C_p^*/C_p)^{1/3}$. For an anisotropic deformation with equal deformation ratios ω_{xy} in two directions and free swelling in the other direction, $\omega = \omega_z = (C_p^*/C_p)/\omega_{xy}^2$. The contribution Π_{mix} from the entropy of mixing is calculated as in the Flory–Huggins/Flory–Rehner theories:[41]

$$\frac{\Pi_{mix}}{RT} = \sum_i C_i - (\ln(1 - C_p\overline{v}_p - C_{pep}\overline{v}_{pep}) + C_p\overline{v}_p + \left(1 - \frac{1}{N}\right)C_{pep}\overline{v}_{pep})/\overline{v}_w \quad (12)$$

where C_i is the concentration of monovalent ion i, $\overline{v}_p$ is the molar volume of a polyion chain segment, C_{pep} is the peptide concentration, $\overline{v}_{pep}$ is the peptide molar volume, N is the peptide degree of polymerization, and $\overline{v}_w$ is the molar volume of water. The contribution to the osmotic pressure in the gel from the electrostatic attraction between network chains (Π_{el}) is assumed to be given by eq 9 also in the presence of the electrolytes specified above. The chemical potentials of the electrolyte containing only monovalent ions (1:1) and that containing peptide (Z:1), respectively, are calculated as

$$\mu_{1:1} = k_B T \ln(C_+C_-) \quad (13)$$

$$\mu_{Z:1} = k_B T \ln(C_{pep}C_-^Z) \quad (14)$$

Equilibrium between the gel and the liquid requires that $\Pi_{mix}^{gel} + \Pi_{el} + \Pi_{def} = \Pi_{mix}^{liq}$, $\mu_{1:1}^{gel} = \mu_{1:1}^{liq}$, and $\mu_{Z:1}^{gel} = \mu_{Z:1}^{liq}$. In addition, both phases must be electroneutral, meaning that the partitioning of ions depends on the degree of dissociation α of the acidic groups on the network. Since the distribution of ions in the gel is assumed to be uniform, α is related to pH in a simple way:

$$\mathrm{pH} = \mathrm{p}K_a + \log\frac{\alpha}{1-\alpha} + \log\frac{C_+^{gel}}{C_{1:1}} \quad (15)$$

where K_a is the acid dissociation constant, C_+^{gel} is the concentration of monovalent cations in the gel, and $C_{1:1}$ is the concentration of 1:1 electrolyte in the liquid. The last term in eq 15 means that all monovalent cations (including H^+) are considered to partition in the same way between the gel and the liquid.

By using the above equations, it is straightforward to find compositions satisfying the equilibrium conditions. For some compositions, these will be satisfied for more than one swelling degree of the gel, indicating the possibility of a gel phase (or volume) transition. In a fluid, the transition would take place at the Maxwell point via a nucleation and growth mechanism. Nucleation of a dense phase in the bulk of a swollen gel is not possible due to an insurmountable elastic energy barrier.[42] However, the gel volume transition can take place once the conditions allow a collapsed layer to form at the gel surface.[43,44] Since the layer is initially infinitely thin, the transition point can be determined by calculating the peptide concentration in the solution required to collapse the network in one direction while keeping the deformation ratios in the perpendicular directions fixed. In addition to the requirement that the core and the shell must be in equilibrium with the liquid phase, phase coexistence in the gel requires that

$$\omega_{xy} = \omega_{core} \quad (16)$$

where ω_{xy} is the deformation of the shell network in the directions parallel to the gel surface and ω_{core} is the deformation ratio of the isotropic core network. The transition takes place when the composition of the liquid is such that

$$\oint \Delta\Pi \, d\omega_z = 0 \quad (17)$$

along the $\Delta\Pi$–ω_z isotherm (at fixed ω_{xy}), where $\Delta\Pi$ is the osmotic pressure difference between gel and liquid and ω_z is the deformation ratio in the direction perpendicular to the gel surface. The requirement in eq 16 leads to a shift of the collapse transition from the Maxwell point to a higher peptide concentration, since the deformation of the shell network is anisotropic and thus in a state of higher elastic energy than an isotropic network of equal composition. In case the conditions for shell formation are never met, the volume change can still be discontinuous at the point of "bulk instability", i.e., when both $\Delta\Pi$ and its derivative with respect to gel volume vanish.

Model Parameters. In all calculations, T = 298 K (l_B = 7.1 Å), $\overline{v}_w = 1.8 \times 10^{-5}$ m^3/mol, pK_a = 4.76, $b = b_0/\alpha$ (b_0 = 2.5 Å),[35] and r = 5.5 Å, the latter representing the bare polyion radius (~3 Å)[35] plus a hydration shell. Unless stated otherwise, the volume per mole of PA chain segments is calculated as $\overline{v}_p = N_A\pi r^2 b_0$, where N_A is the Avogadro number. Furthermore, $\overline{v}_{pep} = 2M\overline{v}_w$, an arbitrary but not unrealistic choice. The parameters describing the elastic free energy of the PA microgels are C_p^* =1.4 M, s = 15, and x = 3.3. The first is set equal to the initial monomer concentration in the polymerization mixture. The other two result from a fit of the model to the pH titration data in Figure 3, representing the set giving the best overall agreement for the studied salt concentrations. Better overall

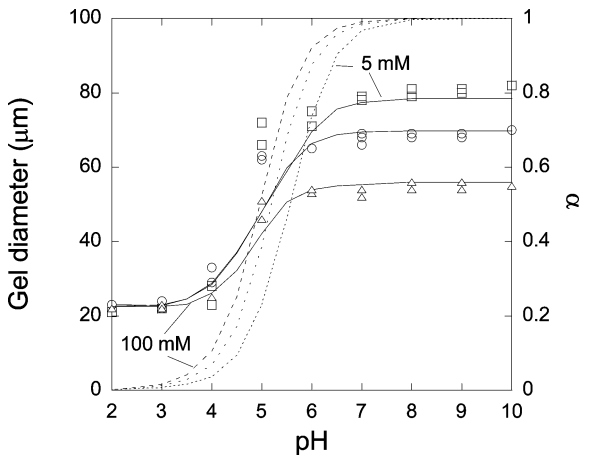

Figure 3. Swelling response of poly(acrylic acid) microgels. Microgel diameter is plotted vs pH in solutions containing 5 (squares), 20 (circles), and 100 (triangles) mM NaCl. Lines are theoretical predictions of microgel diameter (solid) and degree of dissociation α of the network acidic groups (dashed/dotted lines).

dx.doi.org/10.1021/jp306121h | J. Phys. Chem. B 2012, 116, 10964–10975

agreement is also the motive for including the higher order terms in eq 11. Within the theory, the product of s and x equals the average number of monomers in the chains between cross-links. Although we prefer to treat them as material constants related to the structure of the network but not in a simple way, it can be noted that the resulting value of 50 (i.e., 1% degree of cross-linking) is in reasonable agreement with that expected from the amount of cross-linker present during synthesis.

EXPERIMENTAL SECTION

Materials. *N*,*N*′-Methylenebisacrylamide, *N*,*N*,*N*′,*N*′-tetramethyl-ethylenediamine (TEMED), ammonium persulfate, and acrylic acid were obtained from Sigma-Aldrich (Steinheim, Germany), while sorbitan monostearate (Span 60) was from Carl ROTH (Karlsruhe, Germany). The lysine 3-, 5-, and 10-mer oligopeptides (K3, Ac-KKK-NH_2; K5, Ac-KKKKK-NH_2; K10, Ac-KKKKKKKKKK-NH_2) as well as the 10-mer lysine (K)/alanine (A) copeptides (K5A5, Ac-KAKAKAKAKA-NH_2; K3A10, Ac-KAAAKAAAAK-NH_2) were synthesized by Biopeptide Co (San Diego, CA), with a purity confirmed to be >95% by MALDI-TOF MS analysis (Voyager, Applied Biosystems). All other chemicals were of analytical grade.

Microgel Synthesis. Poly(acrylic acid) microgel particles were synthesized by inverse suspension polymerization as described previously.[8] In brief, 0.05 g of Span 60 was dissolved in 20 mL of cyclohexane, and the resulting solution preheated to 45 °C and stirred at 1000 rpm under nitrogen atmosphere. A mixture of 2.6 g of acrylic acid, 0.1 g of *N*,*N*′-methylenebisacrylamide, 20 g of NaOH (2 M), 4 g of NaCl, and 60 μL of TEMED was then prepared. A 10 mL portion of this reaction mixture was mixed with 0.5 mL of 0.18 M ammonium persulfate solution and added to the preheated cyclohexane solution. The polymerization was performed at 65 °C under nitrogen atmosphere to prevent quenching by oxygen. Gelation occurred within minutes, and the reaction was stopped after 30 min by addition of 40 mL of methanol. Gel particles were then left to sediment overnight and then washed repeatedly with methanol and water. Gel particles were sieved using a Retsch 5657 test sieve (Haan, Germany). Fractions below the mesh size of 300 μm were collected and stored in water. The dry mass of these microgels was determined from freeze-drying experiments using a Flexidry μP freeze-dryer (Kinetics Thermal Systems, Stone Ridge, USA).

Volume Response of Single Microgels. The volume change of single poly(acrylic acid) microgels was monitored by micromanipulator-assisted light microscopy, as described previously,[8] using an Olympus Bx-51 light microscope (Olympus, Tokyo, Japan) equipped with an ONM-1 manipulator (Narishige, Tokyo, Japan) and a DP 50 digital camera (Olympus, Tokyo, Japan). Micropipets (~15 μm in diameter) were prepared with a PC-10 puller and a MF-9 forger (both Narishige, Tokyo, Japan). Single microgel particles were captured by micropipet suction using an IM-5A injector (Narishige, Tokyo, Japan), placed inside a 2 mm diameter flow pipet, and flushed with peptide solution using a Peristaltic pump P-1 (Pharmacia, Uppsala, Sweden) at a flow rate of 1 mL/min. Captured microgel particles were photographed using Viewfinder, Studio 3.0.1 (Pixera, San Jose, CA) and the gel-particle diameter measured using Olympus DP-soft (Olympus, Tokyo, Japan).

Volume Change in Response to Salt/pH. To investigate the volume response of microgels at various salt concentrations and pH, a single microgel was captured at pH 7 and salt concentration 20 mM. The gel volume was then measured during pH cycling (pH 7 → pH 10, pH 10 → pH 2, pH 2 → pH 7) at salt concentrations of 5, 20, and 100 mM, respectively. At each condition, the microgel was flushed for at least 5 min, to allow complete equilibration of the gel network. pH was controlled by addition of HCl (2 M) or NaOH (2 M).

Volume change in response to the incorporation of oligopeptides. To investigate the volume response of microgels upon addition of oppositely charged oligopeptides, the volume of a single microgel was investigated in response to increasing peptide monomer concentrations. The gel was equilibrated in each peptide concentration for 30 min (15 min for K5A5 and K3A7), beyond which no further volume change was detectable. After each concentration cycle, before changing to a longer oligolysine, the microgel bound peptides were desorbed by increasing the salt concentration to 200 mM, which caused complete peptide desorption for K3 and K5 (as well as for K5A5 and K3A7). These experiments were performed at various pHs (pH 5 and 8) and salt concentrations (C_s = 5 and 20 mM) in order to evaluate effects of electrostatics on the peptide−microgel interactions. Again, pH was controlled by addition of HCl or NaOH to the solutions.

RESULTS AND DISCUSSION

pH-Dependent Charge and Swelling. Figure 3 shows the equilibrium response of the microgels to variations of pH measured at 5, 20, and 100 mM NaCl. The diameter increases rather abruptly for pH values between 4 and 5 due to dissociation of the acrylic acid groups, the amplitude of the response decreasing with increasing salt concentration. The lines are theoretical curves calculated with a single set of parameters as described above. As can be seen, the calculated pH response is slightly less abrupt than observed experimentally but the variation of the total amplitude of the volume response with the salt concentration is described quite well. Shown also is the calculated degree of dissociation of the network acidic groups, indicating a strong correlation between swelling and charge. An analysis of the force balance underlying the calculated curves reveals that within the entire pH range the contractive force is dominated by that due to network elasticity. However, the repulsive force changes from being completely dominated by the contribution from the polymer entropy of mixing at low pH, where the network is nearly uncharged, to being dominated by the small ion pressure at high pH, where the network is fully charged. The electrostatic attractions contribute little except in a pH range around the apparent pK_a, but the net contribution from charge effects (energy + entropy) is always repulsive, as expected in the weak coupling regime. The failure to fully account for the very abrupt swelling observed experimentally may indicate that the range of the electrostatic (correlation) force is somewhat overestimated. For pH > 4, the volume assigned to the polymer chain has no influence on the calculated curves. This is not the case, however, in the compact states at the lowest pH values where the ionic pressure is so low that the polymer excluded volume interactions come into play. To obtain good agreement with experiments in this range, we put the volume per chain segment equal to that of a water molecule (30 Å^3), corresponding to a cylinder of length 2.5 Å and radius 2 Å. The latter is appropriate for nondissociated poly(acrylic acid) but is lower than the charged cylinder radius used in the calculation of electrostatic energy. No such adjustment is needed in the modeling of the peptide solutions where pH ≥ 5.

Oligopeptides. The results from investigations of the swelling of microgels in oligopeptide solutions are summarized in Figures 4–9. Figure 4a and b shows the dynamics of the

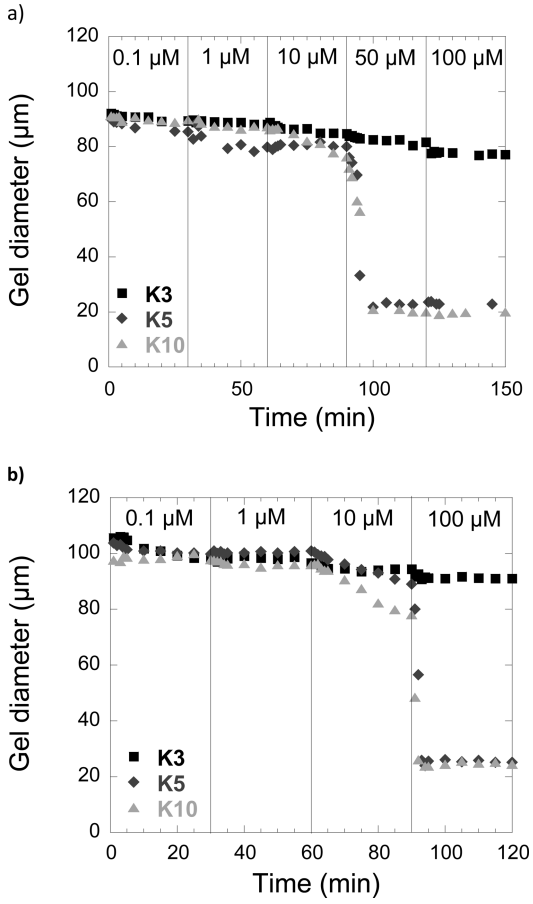

Figure 4. Deswelling kinetics of a single microgel particle with increasing peptide monomer concentration for oligolysine of 3, 5, and 10 repeated units at (a) pH 8, C_s = 5 mM, (b) pH 8, C_s = 20 mM. Peptides were desorbed after each concentration run with 200 mM salt.

deswelling in response to the uptake of oligopeptides K3, K5, and K10 at pH 8 in 5 and 20 mM NaCl, respectively. In these experiments, the concentration of peptide in the liquid flowing around single microgels was increased in steps, monitoring the microgels at each peptide concentration as indicated. The concentrations are expressed as the peptide *monomer* (or, equivalently, charge) concentration in the liquid. The large difference in response observed for K3 and K5, carrying +3 and +5 net charges, respectively, points to a strong dependence on the peptide charge. The small difference between K5 and K10 (+10) is likely to be a nonequilibrium effect related to slow mass transfer to the gel surface. Thus, the collapse in the 50 μM K10 solution (5 μM peptide molecules) at 5 mM salt takes about 10 min, in agreement with what is expected for a stagnant layer diffusion controlled process. A theoretical analysis shows[9] that the time for such a process goes as $1/C_{pep}$, meaning that at concentrations 2 orders of magnitude lower (see below) the relaxation time would be of order 24 h, and therefore difficult to detect in practice (with the present setup). The conclusion is that the diameters observed at the end of each period for peptide concentrations >5 μM molecules (50 μM charges for K10 in Figure 4) can be regarded as equilibrium values but that those for lower concentrations may not be in equilibrium with the liquid, especially not so when attaining that state would require substantial peptide binding.

Figure 5 shows microgel diameters determined after equilibration at pH 8 and 5 mM salt in solutions of K3, K5,

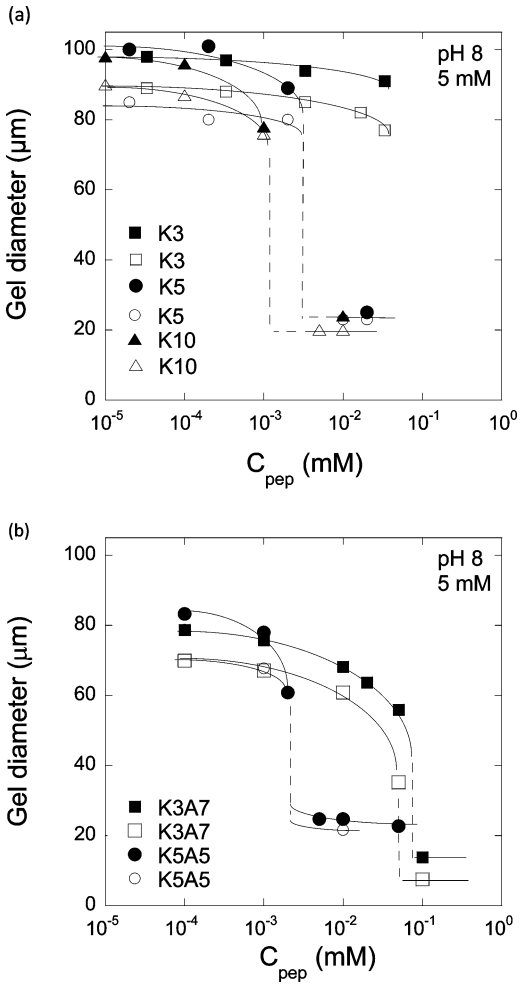

Figure 5. Microgel swelling in peptide solutions, 5 mM salt, pH 8. Microgel diameter plotted vs peptide concentration in the liquid for peptides (a) K3, K5, and K10 and (b) K3A7 and K5A5. Two separate experiments are shown for each peptide. Lines are just guides to the eye.

and K10 (a) and K3A7 and K5A5 (b). Experiments on two different microgel beads were performed for each peptide (filled/open symbols). In all cases where strong deswelling is observed, the process takes place in a narrow concentration range, suggesting that the network undergoes a discrete volume transition. Approximate transitions aimed as guides to the eye are indicated by dashed lines in the graphs. We stress, however, that more data points would be needed to discriminate between such a transition and a sharp yet continuous process (see below). The effect of increasing the peptide charge density is strong, most clearly seen when comparing K3A7 and K5A5. Importantly, the minor effect of increasing N from 5 to 10 by incorporating uncharged monomers between the charged monomers in the chain, as evident from a comparison between K5 and K5A5, indicates that the total charge of the peptide is more important than the charge density. From this and the fact that K3A7 induces a strong volume change, it is likely that also

dx.doi.org/10.1021/jp306121h | J. Phys. Chem. B 2012, 116, 10964–10975

the K3 curve should start to drop at a concentration slightly larger than the highest one investigated.

The results from the theoretical modeling of the systems are shown in Figure 6. The diameter in peptide-free solution is set to 85 μm (in the calculations, the size does not affect the state of the gel). The transition changes from continuous to discontinuous as the charges of the model chains are increased from +2 to +3. By allowing a continuous variation of the charge for chains with N = 10 (solid lines), a crossover between these regimes is found at +2.3 (β = 0.86, C_{pep} = 2.2 mM). The result for a chain with a charge just below that value is included to highlight the difficulty of distinguishing between continuous and discontinuous volume changes.

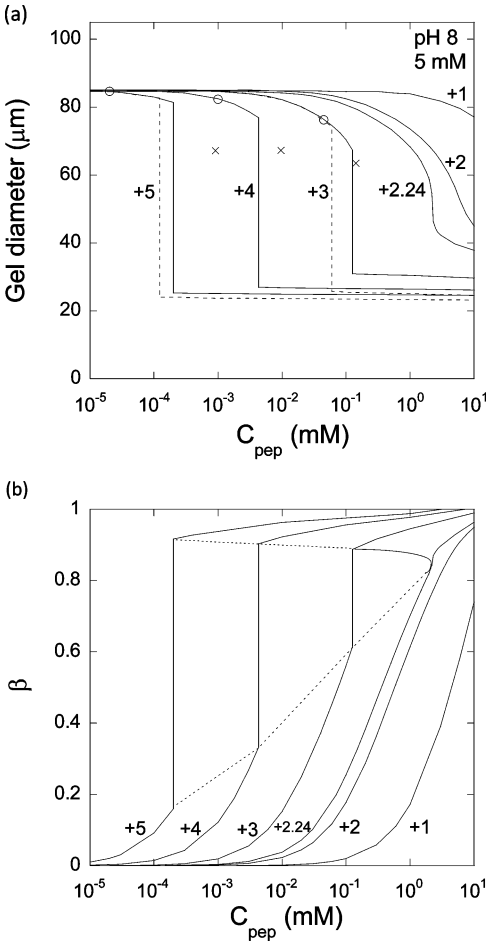

Figure 6. (a) Theoretically calculated swelling isotherms for microgels in solutions of peptides with charge numbers (Z) as indicated; 5 mM salt, pH 8, N = 10 (solid lines), N = Z (dashed lines). Circles, Maxwell points (N = 10); crosses, bulk instability points (N = 10). (b) Theoretically calculated binding isotherms for microgels in solutions of peptides with charge numbers (Z) as indicated; 5 mM salt, pH 8, N = 10, gel diameter in peptide-free liquid = 85 μm. Dashed line: Approximate boundary between collapsed and swollen states for a continuous variation of peptide charge.

In agreement with experiments, the effect of incorporating noncharged segments in the peptide chains is minor, as shown by the results obtained with N equal to 3 and 5 for charge numbers +3 and +5, respectively (Figure 6a, dashed lines). The shifts of the transition concentrations are explained by the contribution from the uncharged segments to the entropy of mixing giving rise to a higher swelling pressure, resulting also in slightly larger gel diameters of the collapsed state.

All calculated discrete transitions follow the core/shell route to collapse. On each curve for the N = 10 chains, the Maxwell transition point is indicated by a circle, and in the extension of the swollen branch, the point where bulk instability would have occurred is indicated by a cross. With decreasing peptide charge, the relative position of the core/shell transition shifts closer to the point of bulk instability to nearly coincide with that for the +3 chain.

The attractive electrostatic component of the model is needed both to reproduce the dense packing of the molecules in the collapsed state observed experimentally and for the discrete transitions to occur. Thus, within the model, the network elastic force alone, while favoring a collapsed state, is not strong enough to produce these effects.

The calculated transition concentration for the +3 chain (N = 10) is in good agreement with the concentration where strong deswelling occurs for K3A7. The transition concentration decreases rapidly with increasing peptide charge, but the calculated effect is larger than that observed experimentally. Within the model, the shift reflects largely the influence of charge on the binding strength where the gain in entropy (per bound peptide) from creating a more uniform distribution of counterions in the system increases with increasing peptide charge. The calculated binding isotherms are given in Figure 6b, where the peptide/network charge ratio (β) is plotted vs C_{pep} in the liquid. At low binding ratios, the isotherms are shifted to lower concentration by approximately one decade per added charge, consistent with a binding constant increasing approximately as K^Z, as suggested earlier for protein binding to colloidal microgels.[45] The dashed curve in Figure 6b shows approximately the boundary of the core/shell coexistence region for a continuous variation of the peptide charge with a critical point to the right.

To understand what determines the transition concentration, it is instructive to look at the contributions to the osmotic pressure. These are shown in Figure 7 as a function of volume per mole of segments in the network (V) for the case of Z = +3, N = 10. The corresponding graphs for chains with higher charge have the same qualitative features (not shown). Figure 7a shows the situation at the Maxwell concentration where the collapsed and swollen states are in thermodynamic equilibrium. The volumes of these are given by the outermost points where the total osmotic pressure difference between gel and liquid (thick solid line) equals zero. The volume of the swollen state is determined by a balance between the swelling pressure from entropy of mixing, largely dominated by the contribution from the small ions, and the attractive pressure due to elastic deformations and electrostatic attractions, where the former dominates. In the collapsed state, the electrostatic attractions and the entropy of mixing give by far the largest contributions. Here the entropy of mixing is dominated by the contributions from the peptide and network chains (where excluded volume effects are taken into account on the Flory–Huggins level). The ion pressure is small because the network charges are largely neutralized by the peptides (β = 0.89). The elastic pressure is small, but the electrostatic and mixing pressures largely balance each other; hence, its contribution is of the same order of magnitude as the difference between them. Despite this, it has only very minor effects on the shape of the total osmotic pressure curve and the composition in the collapsed state because it is almost invariant in the relevant range.

dx.doi.org/10.1021/jp306121h | J. Phys. Chem. B 2012, 116, 10964–10975

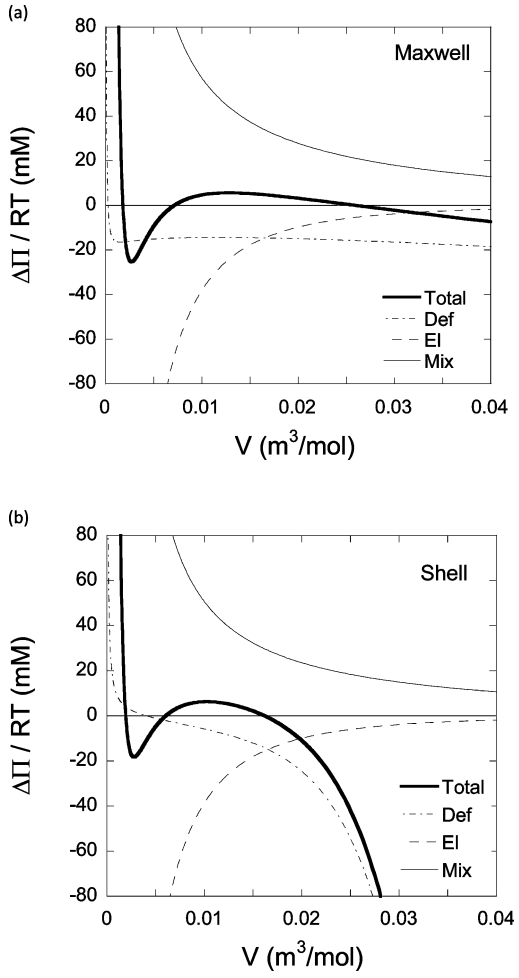

Figure 7. Calculated total and individual contributions to the osmotic pressure difference between gel and liquid ($\Delta\Pi$) as functions of gel volume per mole of monomers in the network (V) at (a) the Maxwell point and (b) the shell transition point; Z = +3, N = 10, 5 mM salt, pH 8. Key to contributions: Tot = total osmotic pressure, Def = elastic deformation energy, El = electrostatic energy, mix = entropy of mixing (network + peptide + small ion).

For a given composition of the liquid, the state of the system is completely determined by the state of the network, and the most favorable state determined by a balance between energy and entropy. The attractive electrostatic force makes the collapsed state stable against osmotic swelling already at peptide concentrations in the liquid far below the Maxwell concentration. However, in this range, it is only metastable because the gain in energy and entropy from recruiting peptides from the liquid is not enough to compensate for the entropic loss of confining the molecules to the compact state. For a given degree of swelling, the partitioning of peptide is determined only by entropy (within the model). The peptide/network charge ratio in that state increases with increasing peptide concentration in the liquid. The resulting lower swelling pressure from the small ions allows the network to reach a more compact state of lower electrostatic (and elastic) energy. At the Maxwell point, the peptide concentration in the liquid is large enough to make the total entropic cost equal to the gain in energy, so the collapsed and swollen states are in thermodynamic equilibrium. The total entropic cost is small in general because the ion exchange of network counterions increases the small ion entropy in the system. This explains the low peptide concentration needed to reach the Maxwell point and why this concentration decreases with increasing peptide charge. A related effect is the lowering of the Maxwell concentration with increasing degree of cross-linking of the network (not shown). The reduced swelling increases the charge concentration in the network, increasing the entropic driving force of replacing counterions, and therefore allows a high peptide/network charge ratio to be reached at a lower peptide concentration. This effect dominates over the gain in elastic energy for the collapse process.

As already pointed out, in gels, the transition at the Maxwell point is prohibited. Instead, bulk instability is expected at the concentration where the maximum of the total pressure curve in the loop is suppressed to zero. However, prior to that, shell formation becomes favorable in the present system. Figure 7b shows the situation in the shell at the shell transition point. Note that on the abscissa is plotted the volume of the shell (per moles of segments in the network) not the gel volume. Due to the fixed lateral strain imposed on the shell network, deformation is only allowed in one direction. This gives rise to a stronger variation of the elastic pressure with volume compared to the isotropic case, and in the collapsed shell, the elasticity actually promotes swelling. At higher volumes, it resists swelling but the pressure is less negative than in the isotropic state, so the collapse is less promoted by the elasticity. This means a larger degree of peptide binding is needed to bring down the swelling pressure to the level where the collapsed phase is in equilibrium with the swollen core, explaining why the transition takes place at a higher concentration than at the Maxwell point. (An equivalent, but complementary, interpretation is given in the Theory section.) Another effect of the weaker collapsing force in the shell is that the swelling is slightly larger than in the collapsed isotropic state. At the transition concentration, the concentration of network charges in the first thin shells formed is 0.52 and 1.03 M for Z = +3 and +5 (N = 10), respectively. The corresponding values for the collapsed isotropic states reached when the transition is completed are 0.58 and 1.06 M, respectively. The peptide/network charge ratios are practically unchanged and similar for the two peptides. The swelling decreases with increasing peptide charge, since the contribution to the swelling pressure from the peptide entropy of mixing decreases. Elastic effects are small because the elastic force in the collapsed state is very small compared to electrostatic force. Nevertheless, the elevated elastic energy of the stretched-out network makes the core/shell gel state unstable against the collapsed isotropic state. In a more elaborate investigation of the binding of charged spheres (from a reservoir) to oppositely charged networks, it is shown[46] that once the first shell is formed the transition proceeds to the collapsed isotropic state via intermediate core/shell states. Other effects of peptide charge and degree of cross-linking are the same as at the Maxwell transition point.

Salt Effect. The effect of increasing the salt concentration to 20 mM at pH 8 is shown in Figure 8 together with the theoretical results for these systems. At the elevated salt concentration, no collapse is observed for K3 and K5 in the studied range, but the data for K5 shows that the transition (if it occurs) must be shifted by at least 1 order of magnitude to higher peptide concentrations. The calculated curve for Z = +5 has a discrete core/shell transition also in this case, and the transition concentration is shifted about 3 orders of magnitude from that at 5 mM salt. For Z = +3, a bulk instability transition

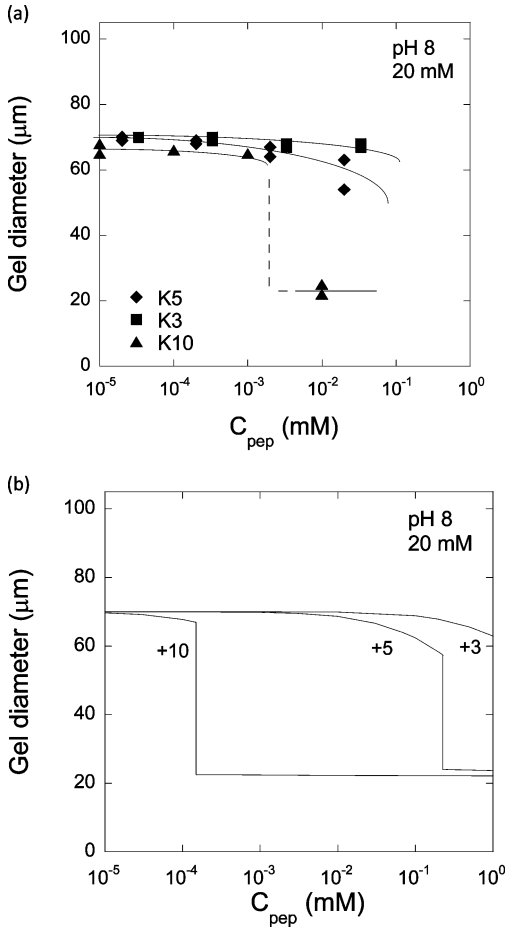

Figure 8. (a) Microgel swelling in peptide solutions, 20 mM salt, pH 8. Microgel diameter plotted vs peptide concentration in the liquid for peptides K3, K5, and K10. Lines are just guides to the eye. (b) Theoretically calculated swelling for the conditions in part a; gel diameter in peptide-free liquid = 70 μm.

(not shown) takes place at 5.6 mM. The shift is about 1 order of magnitude smaller than for Z = +5. Increasing the salt concentration reduces the peptide binding strength to the gel, since the entropic driving force from releasing network counterions becomes smaller. However, salt should also screen the charge interactions in a more direct way. In the model, this is accounted for by the salt dependence of the model parameter y_0, determined by PB calculations. Through this parameter, the electrostatic attractions in the gel decrease with increasing salt, reducing the driving force for phase transition. The calculations show that both effects contribute significantly to the shift of the transition concentrations for the peptides with $Z = N = 3$ and $Z = N = 5$. Increasing N to 10 for the former changes the transition from discontinuous to continuous, showing that the balance between entropy and energy is delicate and that small variations can even change the behavior qualitatively.

The collapse concentration for K10 does not seem to deviate much from that at 5 mM salt. The result would be highly unexpected at equilibrium considering the effects of salt just discussed. Clearly, the transition at 5 mM salt for this peptide is kinetically hindered by slow mass transfer to the gel. The concentration where the volume change takes place for K10 in Figure 5 is in agreement with the lowest one for which the mass transfer rate is expected to match the observation time.[9]

pH Effect. Swelling isotherms at pH 5 in 5 mM salt are shown in Figure 9. For the peptides with lowest and highest

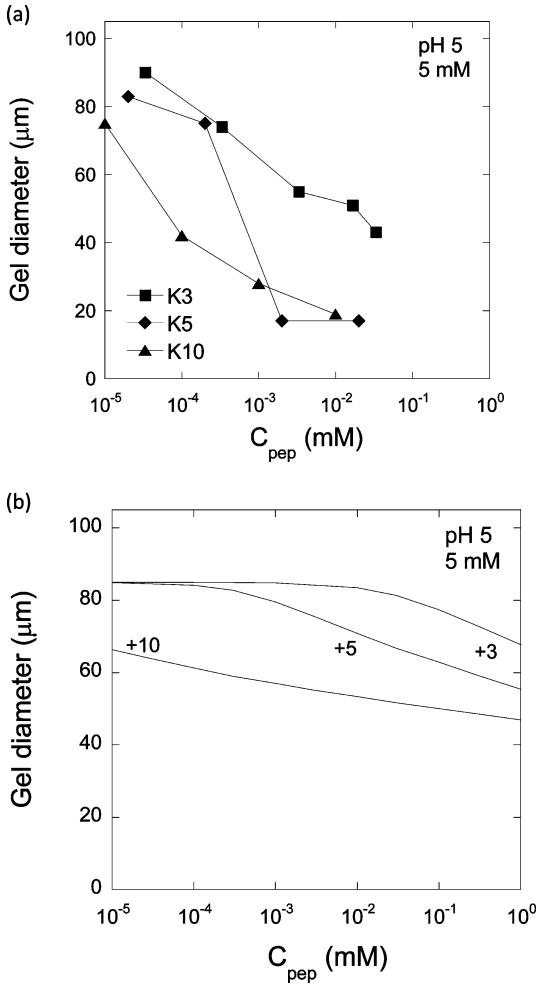

Figure 9. (a) Microgel swelling in peptide solutions, 5 mM salt, pH 5. Microgel diameter plotted vs peptide concentration in the liquid for peptides K3, K5, and K10. Lines are just guides to the eye. (b) Theoretically calculated swelling for the conditions in part a; gel diameter in peptide-free liquid = 85 μm.

charge, the gel diameter clearly changes more gradually as a function of peptide concentration than at the higher pH. For the intermediate one, a stronger dependence is observed. The peptide charge numbers should be unaffected by the pH change, but the degree of dissociation of the carboxylic acid groups on the network is expected to decrease with decreasing pH (cf. Figure 3). The latter effect, lowering the electrostatic coupling, is consistent with the less dramatic volume changes observed. However, the reduction of the gel diameter is substantial for all peptides in the studied range of peptide concentrations and for K3 even larger than at pH 8. This is not surprising, since the networks respond to lowering of the linear charge density by decreasing the swelling already in the absence of peptide, thereby maintaining a high charge concentration and a large entropic driving force for peptide binding. The latter interpretation is supported by the calculations underlying the theoretical curves in Figure 3, showing that the concentration of network charges at pH 5 is as large as 82% of that at pH 8.

dx.doi.org/10.1021/jp306121h | J. Phys. Chem. B 2012, 116, 10964−10975

The theoretical swelling isotherms for pH 5 are shown in Figure 9b. The results are in qualitative agreement with the experiments, but the volume responses are underestimated. Analysis of the contributions to the osmotic pressure shows that the attractive electrostatic component is much reduced by the pH change, explaining why no volume transition takes place despite the fact that the peptide binding effectively reduces the small ion swelling pressure. Interestingly, peptide binding is accompanied by charge regulation of the network. For instance, the degree of dissociation of the acidic groups changes from 0.27 to 0.39 as the peptide concentration in the liquid increases from zero to 0.1 mM for the $Z = +5$ ($N = 5$) peptide. Charge regulation is a way for the system to lower the free energy, facilitating binding at high binding ratios.

Multivalent Ions. The theoretical calculations show that peptides with sufficiently high charge should induce volume transitions of the networks. The experimental results support this but do not prove that the volume change is discontinuous. More clear-cut evidence can be found in the literature on charged networks interacting with multivalent inorganic ions.[47] Figure 10a shows the effect of various salts on the swelling of NaPA networks in aqueous solution, as reported by Horkay and co-workers.[48] The inverse volume fraction of polymer $1/\varphi$ (proportional to the gel volume) is given as a function of the concentration of multivalent salt added to a 40 mM NaCl solution. The differences seen between different divalent salts reveal ion specific effects. However, for all, a discrete volume change takes place already at a low concentration, and for the trivalent salt, the transition concentration is even smaller. In contrast, adding more NaCl (top curve/scale) produces no transition. The observed effects are reproduced quite well by the theoretical model, as evident from Figure 10b. The network volume fraction is very high even in the most swollen state, indicating that the gels are substantially more cross-linked than the microgels used by us. This was modeled by reducing the network elasticity parameter s to 2.7, a value giving approximately the same polymer volume fraction in the gel in 40 mM NaCl as in the experiments. Due to the high counterion concentration in the gel already at this ionic strength, the concentration difference between gel and liquid changes too little upon further NaCl addition to have a strong effect on the swelling pressure. In combination with a weaker elastic force at a lower degree of swelling, this explains the small response to NaCl addition in the studied range. Interestingly, the theoretical curve (+1; top scale) has a maximum near 60 mM salt. This is a result of a competition between two effects of increasing the concentration of simple salt, the one promoting deswelling by increasing the osmotic pressure in the liquid, the other promoting swelling by screening the electrostatic attractions in the gel. The maximum appears only for highly cross-linked networks, where, even at low salt concentration, the polyion chains are close together so that the electrostatic (correlation) attraction comes into play. In weakly cross-linked networks, the salt dependence is monotonic, since reducing the elastic force shifts the osmotic balance point to higher degrees of swelling, where the electrostatic attraction is weaker.

The dramatic effects of adding small amounts of di- and trivalent cations are quite analogous to the ones of adding multivalent peptide chains to the microgels, and they are explained by the theory in a similar way. However, the transitions are found to take place at the point of bulk instability. It should be mentioned that, in order to isolate the effect of the charge of the small ions, their volumes are set to zero, as is the volume of the monovalent ions in all calculations. The composition of the collapsed state and therefore the transition point are then strongly influenced by the excluded volume interactions among the hydrated network chains. The curves shown were obtained with a volume per monomer corresponding to a cylinder of length 2.5 Å and radius 4.0 Å, the latter value only slightly smaller than that used in the calculations of the peptide systems.

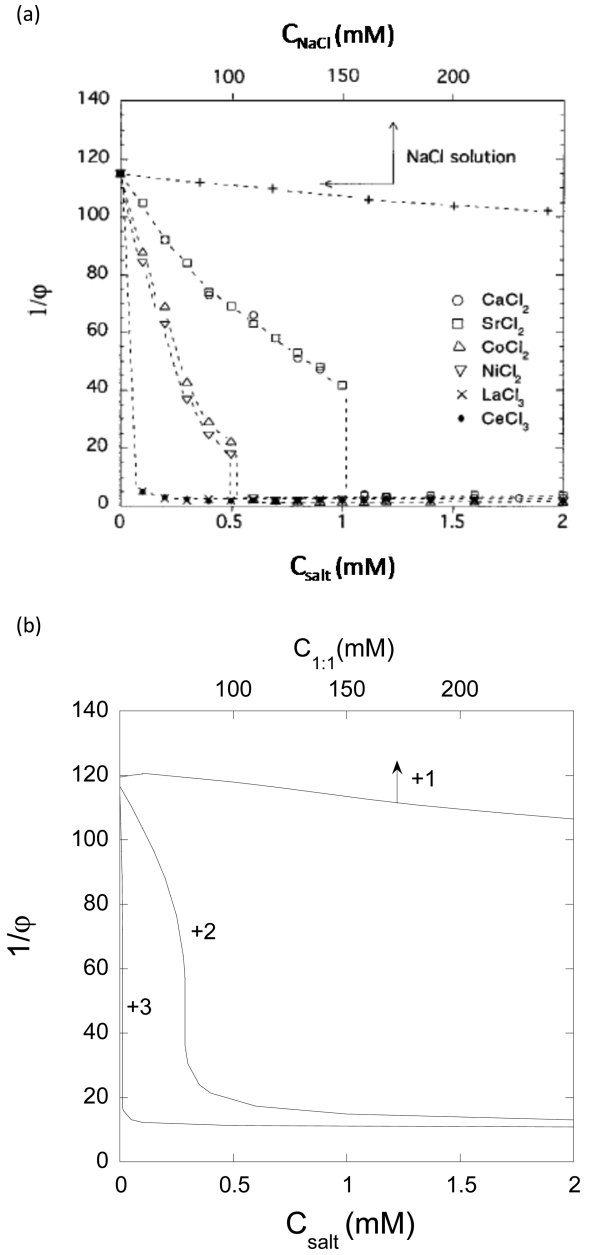

Figure 10. Effect of multivalent inorganic salt ions on the swelling of PA gels in 40 mM NaCl. (a) Experimental results for various salts. Adapted from ref 48. Top curve/scale: addition of NaCl. (b) Theoretical modeling of the systems in part a. Charge number of salt cations as indicated in the graph.

CONCLUSIONS

By micromanipulator-assisted light microscopy, the equilibrium volume response of single poly(acrylic acid) microgel particles upon pH and ionic strength variations, as well as of concentration-, length-, and charge-density-dependent peptide

dx.doi.org/10.1021/jp306121h | J. Phys. Chem. B 2012, 116, 10964−10975

absorption, could be successfully monitored. Results show that the tendency of the peptides to induce microgel deswelling increases with peptide length and charge density. Furthermore, the oligolysine uptake was reduced at pH 5 compared to at pH 8, in agreement with the reduced microgel charge content at the lower pH. Microgel deswelling response, however, was more pronounced at low pH, as lower oligomer concentrations were required to induce significant microgel deswelling, in agreement with the lower microgel network charge density at pH 5. Theoretical modeling based on charge interactions between peptide and network, excluded volume interactions, and elastic stress in the microgels was able to semiquantitatively capture these effects, and indicated the importance of peptide charge (length) rather than peptide charge density for causing microgel network deswelling. The model furthermore predicts a transition from continuous network deswelling to a discrete collapse at a critical net charge of the binding species, in agreement with both results obtained in the present investigation, and with results in the literature on gel deswelling as a function of counterion valency. Taken together, the present results demonstrate the importance of ion exchange in highly charged peptide/microgel systems but also that such effects can be modeled by the presented considerations of electrostatic interactions and network elasticity, thus facilitating the application of microgels as delivery systems for highly charged peptide drugs.

AUTHOR INFORMATION

Corresponding Author

*E-mail: per.hansson@farmaci.uu.se.

Notes

The authors declare no competing financial interest.

ACKNOWLEDGMENTS

Dr. Maarten Biesheuvel is gratefully acknowledged for stimulating early discussions on this project, and Jonas Gernandt for fruitful discussions throughout the project. This work was financed by the Swedish Research Council.

REFERENCES

(1) Kabanov, A. V.; Vinogradov, S. V. *Angew. Chem., Int. Ed.* **2009**, *48*, 5418−5429.
(2) Vinogradov, S. V. *Curr. Pharm. Res.* **2006**, *12*, 4703−4712.
(3) Malmsten, M.; Bysell, H.; Hansson, P. *Curr. Opin. Colloid Interface Sci.* **2010**, *15*, 435−444.
(4) Hoare, T.; Pelton, R. *Biomacromolecules* **2008**, *9*, 733−740.
(5) Bromberg, L.; Temchenko, M.; Alakhov, V.; Hatton, T. A. *Langmuir* **2005**, *21*, 1590−1598.
(6) Zhang, Y.; Zhu, W.; Wang, B.; Ding, J. *J. Controlled Release* **2005**, *105*, 260−268.
(7) Bysell, H.; Malmsten, M. *Langmuir* **2009**, *25*, 522−528.
(8) Bysell, H.; Malmsten, M. *Langmuir* **2006**, *22*, 5476−5484.
(9) Bysell, H.; Hansson, P.; Malmsten, M. *J. Phys. Chem. B* **2010**, 7207−7215.
(10) Bysell, H.; Schmidtchen, A.; Malmsten, M. *Biomacromolecules* **2009**, *2009*, 2162−2168.
(11) Wong, E.; Diez-Pascual, A. M.; Richtering, W. *Macromolecules* **2009**, *42*, 1229−1238.
(12) Kleinen, J.; Klee, A.; Richtering, W. *Langmuir* **2010**, *26*, 11258−11265.
(13) Bysell, H.; Hansson, P.; Schmidtchen, A.; Malmsten, M. *J. Phys. Chem. B* **2010**, *114*, 1307−1313.
(14) Haynie, D. T.; Zhao, W. *J. Nanosci. Nanotechnol.* **2009**, *9*, 3562−3567.
(15) Diez-Pascual, A. M.; Wong, J. E. *J. Colloid Interface Sci.* **2010**, *347*, 79−89.
(16) Johansson, C.; Hansson, P.; Malmsten, M. *J. Phys. Chem. B* **2009**, *113*, 6183−6193.
(17) Månsson, R.; Bysell, H.; Hansson, P.; Schmitdchen, A.; Malmsten, M. *Biomacromolecules* **2011**, *12*, 419−424.
(18) Nilsson, P.; Hansson, P. *J. Phys. Chem. B* **2005**, *109*, 23843−23856.
(19) Bodrova, A. S.; Potemkin, I. I. *Polym. Sci., Ser. A* **2007**, *49*, 737−744.
(20) Hansson, P. *Curr. Opin. Colloid Interface Sci.* **2006**, *11*, 351−362.
(21) Hansson, P. *J. Phys. Chem. B* **2009**, *113*, 12903−12915.
(22) Hua, J.; Mitra, M. K.; Muthukumar, M. *J. Chem. Phys.* **2012**, *136*, 134901.
(23) Yin, D.-W.; M., O. d. l. C.; de Pablo, J. J. *J. Chem. Phys.* **2009**, *131*, 194907.
(24) Moreira, A. G.; Netz, R. R. *Phys. Rev. Lett.* **2000**, *87*, 078301.
(25) Naji, A.; Jungblut, S.; Moreira, A. G.; Netz, R. R. *Physica A* **2005**, *352*, 131−170.
(26) Evans, F.; Wennerström, H. *The Colloidal Domain: where Physics, Chemistry, Biology, and Technology Meet*; VCH Publishers: New York, 1994.
(27) Henderson, D.; Blum, L. *J. Chem. Phys.* **1978**, *69*, 5441.
(28) Wennerström, H.; Jönsson, B.; Linse, P. *J. Chem. Phys.* **1982**, *76*, 4665−4670.
(29) Jönsson, B.; Wennerström, H. *J. Adhes.* **2004**, *80*, 339−364.
(30) Samaj, L.; Trizac, E. *Phys. Rev. Lett.* **2011**, *106*, 078301.
(31) Chen, Y.-G.; Weeks, J. D. *Proc. Natl. Acad. Sci. U.S.A.* **2006**, *103*, 7560−7565.
(32) Santangelo, C. D. *Phys. Rev. E* **2006**, *73*, 041512.
(33) Nordholm, S. *Chem. Phys. Lett.* **1984**, *105*, 302−307.
(34) Forsman, J. *J. Phys. Chem. B* **2004**, *108*, 9236−9245.
(35) Gunnarsson, G.; Gustavsson, H. *J. Chem. Soc., Faraday Trans. 1* **1982**, *78*, 2901−2910.
(36) Leal, C.; Moniri, E.; Pegado, L.; Wennerström, H. *J. Phys. Chem. B* **2007**, *111*, 5999−6005.
(37) Biesheuvel, P. M. *Langmuir* **2004**, *20*, 4764−4770.
(38) Jönsson, B.; Wennerström, H. *J. Phys. Chem.* **1987**, *91*, 338−352.
(39) Treloar, L. R. G. *Rep. Prog. Phys.* **1973**, *36*, 755−826.
(40) Hasa, J.; Ilavský, J.; Dušek, K. *J. Polym. Sci., Polym. Phys.* **1975**, *13*, 253−262.
(41) Flory, P. J. *Principles of polymer chemistry*; Cornell University Press: Ithaca, NY, 1953.
(42) Onuki, A. *Phys. Rev. A* **1988**, *38*, 2192−2195.
(43) Sekimoto, K. *Phys. Rev. Lett.* **1993**, *70*, 4154−4157.
(44) Tomari, T.; Doi, M. *Macromolecules* **1995**, *28*, 8334−8343.
(45) Johansson, C.; Gernandt, J.; Bradley, M.; Vincent, B.; Hansson, P. *J. Colloid Interface Sci.* **2010**, *347*, 241−251.
(46) Gernandt, J.; Hansson, P. Submitted.
(47) Tanaka, T. *J. Chem. Phys.* **1982**, *77*, 5725−5729.
(48) Horkay, F.; Tasaki, I.; Basser, P. J. *Biomacromolecules* **2001**, *2*, 195−199.